Archetypal energy landscapes

David J. Wales, Mark A. Miller & Tiffany R. Walsh

University Chemical Laboratories, Lensfield Road, Cambridge CB2 1EW, UK

Energy landscapes hold the key to understanding a wide range of molecular phenomena. The problem of how a denatured protein re-folds to its active state (Levinthal's paradox[1]) has been addressed in terms of the underlying energy landscape[2–7], as has the widely used 'strong' and 'fragile' classification of liquids[8,9]. Here we show how three archetypal energy landscapes for clusters of atoms or molecules can be characterized in terms of the disconnectivity graphs[10] of their energy minima—that is, in terms of the pathways that connect minima at different threshold energies. First we consider a cluster of 38 Lennard–Jones particles, whose energy landscape is a 'double funnel' on which relaxation to the global minimum is diverted into a set of competing structures. Then we characterize the energy landscape associated with the annealing of C_{60} cages to buckminsterfullerene, and show that it provides experimentally accessible clues to the relaxation pathway. Finally we show a very different landscape morphology, that of a model water cluster $(H_2O)_{20}$, and show how it exhibits features expected for a 'strong' liquid. These three examples do not exhaust the possibilities, and might constitute substructures of still more complex landscapes.

We use disconnectivity graphs[10] to visualize the energy landscapes, based upon samples of pathways linking local minima via transition states. At any given total energy we elucidate which of the local minima in our sample are connected by pathways that lie below the energy threshold. At finite energy the minima are divided into disconnected sets of mutually accessible structures, separated by insurmountable barriers. The resulting graphs are clearest when we present the results as the total energy increases in regular steps along the vertical axis. Each line begins from a different local minimum at a vertical height determined by the potential energy at the bottom of the corresponding well. A node joins lines at the lowest energy for which the minima become mutually accessible. We are free to choose the horizontal displacements to give the most helpful representation of the resulting graph.

Graphs such as these, which are connected but contain no cycles, are known as 'trees' for reasons which should be clear from Fig. 1. The gentle 'funnel' with high barriers in Fig. 1a produces a graph which looks like a weeping willow. The graph for the efficient funnel with lower barriers in Fig. 1b reminds us of a palm tree, whilst the graph for the rough landscape in Fig. 1c resembles a banyan tree with its branches planted into the ground.

We first focus on a cluster of 38 atoms bound by the Lennard–Jones potential, represented here by $(LJ)_{38}$. The lowest-energy icosahedral minimum lies significantly above the truncated octahedron[11], and the two minima are well separated in configuration space. Relaxation to the global minimum is hampered because the vast majority of local minima are associated with the liquid-like state of the cluster and have polytetrahedral character[11]. Minima based upon icosahedra also have polytetrahedral character, but the truncated octahedron is a fragment of close-packed lattice.

Hence the $(LJ)_{38}$ cluster provides a pattern for the 'double funnel'

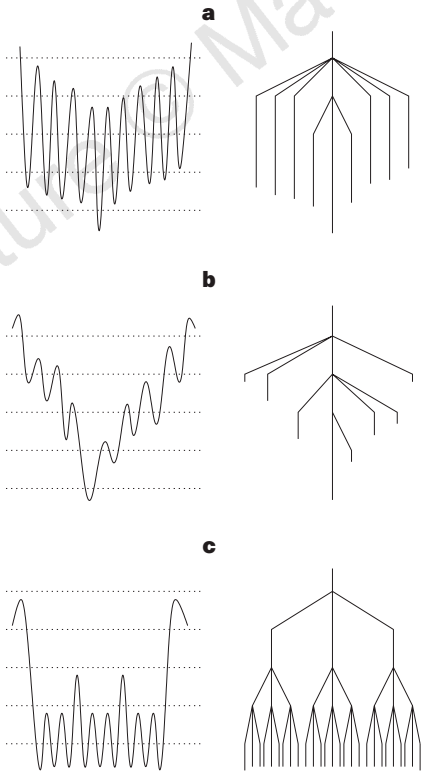

Figure 1 Pictorial correspondence between the potential-energy surface and the disconnectivity graph for three different energy landscapes, following Becker and Karplus[10]. **a**, The 'weeping willow' results from a gentle funnel with large barriers. **b**, The 'palm tree' results from a steeper funnel with lower barriers. **c**, The 'banyan tree' results from a rough landscape.

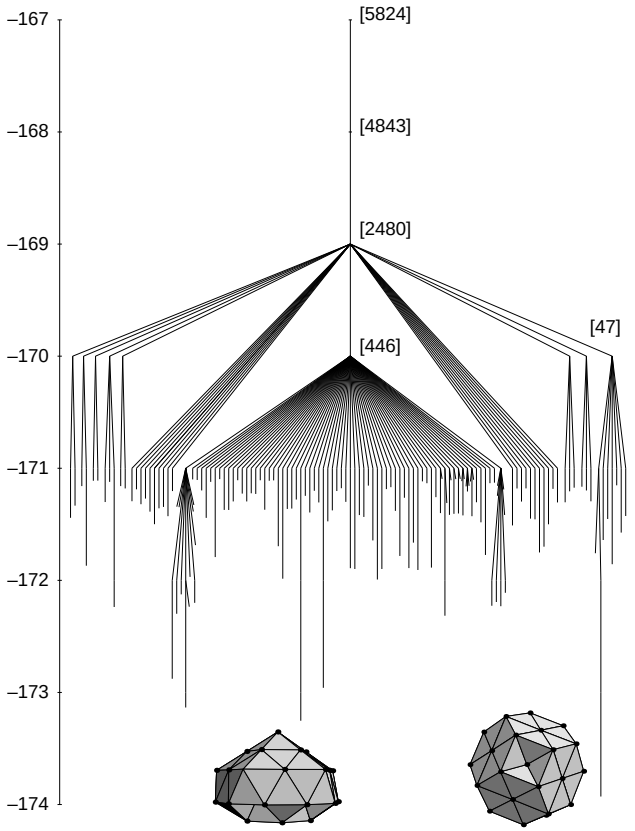

Figure 2 Disconnectivity graph for the double-funnel surface of $(LJ)_{38}$. The energy on the vertical axis is measured in terms of the pair well depth. The numbers in square brackets indicate the number of minima represented by the adjacent node; only branches leading to the lowest 150 minima are shown explicitly.

surface, and understanding the dynamics of this system should provide insight into landscapes which support competing morphologies. Our sample of stationary points for $(LJ)_{38}$ contains 6,000 minima and 8,633 transition states, along with the corresponding pathways. The construction of such databases has been described before[2,12] and the resulting graph is shown in Fig. 2. For clarity we have removed branches that do not lead to the lowest 150 minima. The graph shows that of these minima, most lie in the region of configuration space associated with icosahedra, rather than with the global minimum. Hence, relaxation to the global minimum is diverted by the presence of a competing morphology associated with a much larger region of configuration space and higher entropy.

We next turn to C_{60}. A number of studies[13–21] have proposed mechanistic schemes to explain the formation of buckminsterfullerene, but simulations of fullerene nucleation usually produce defective structures[22–27]. The exceptions are a calculation starting from the adjacent local minimum[28] and a study where the dynamics appear to be accelerated because the potential employed has rather low barriers[29]. For potentials which support realistic barriers, the timescale for fullerene annealing lies beyond the reach of traditional simulation techniques. The present calculations employed a semi-empirical, quantum-mechanical tight-binding potential[30].

We have deduced the disconnectivity graph for C_{60} using the most likely annealing mechanism, assuming that a C_{60} molecule with 12 pentagonal and 20 hexagonal faces has already been reached somehow, and neglecting fullerenes with square or heptagonal faces. This approach seems reasonable, as both the 'pentagon road' and 'hexagon road' growth mechanisms entail annealing after the formation of higher-energy C_{60} fullerene isomers[14–16].

Excluding enantiomers, there are 1,812 different isomers for C_{60} with 12 pentagonal and 20 hexagonal faces, and following Austin *et al.*[31] we have performed geometry optimizations for all these minima. Austin *et al.*[32] have also investigated the connectivity of the same set of minima under a generic rearrangement mechanism proposed by Stone and Wales[33]. This 'pyracylene' or 'Stone–Wales' mechanism provides a means for pentagonal and hexagonal rings to migrate over the surface of the cluster. The

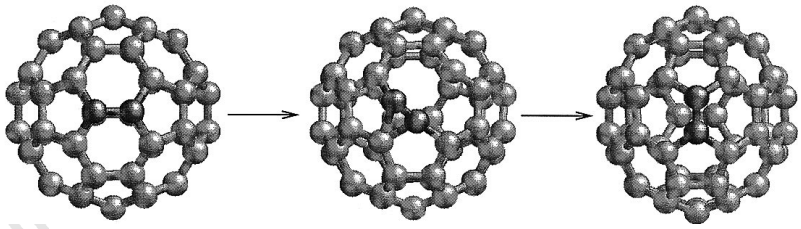

Figure 3 The 'pyracylene' or 'Stone–Wales' rearrangement of C_{60}. Buckminsterfullerene, left, is transformed via the transition state, centre, to give the new C_{2v} symmetry minimum, right.

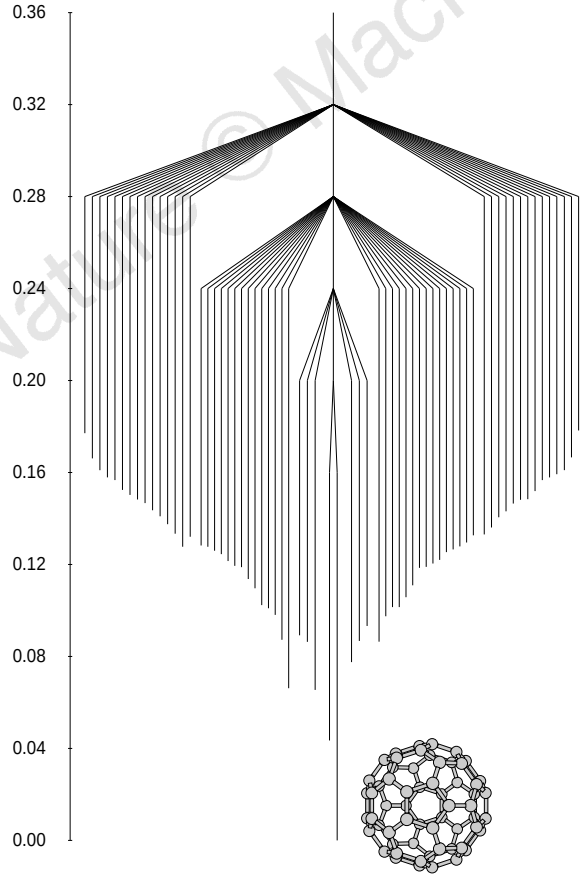

Figure 4 Disconnectivity graph for minima and transition states in the five lowest Stone–Wales stacks of C_{60}. Energy is in hartrees relative to the global minimum buckminsterfullerene structure.

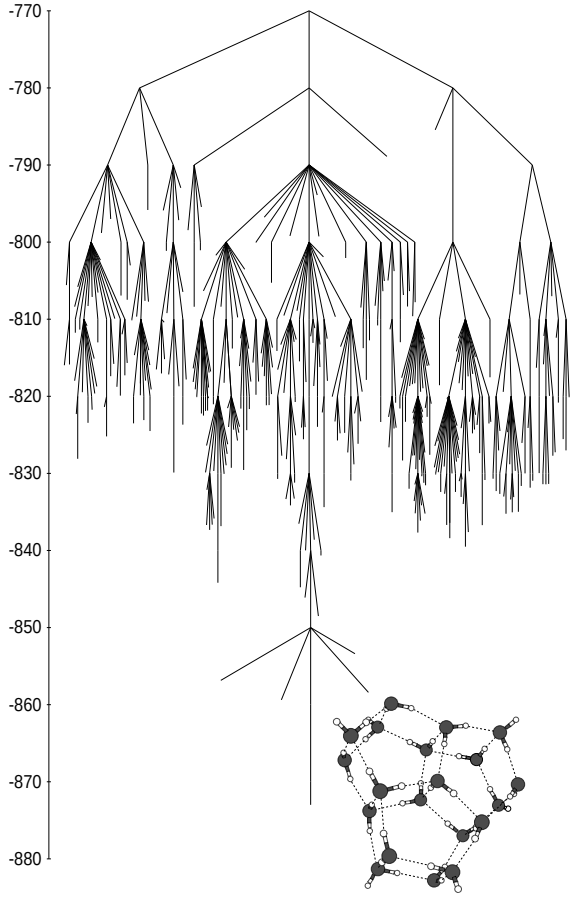

Figure 5 Disconnectivity graph for a sample of minima and transition states around the global minimum of the TIP4P $(H_2O)_{20}$ cluster. Energy is in kJ mol^{-1}.

transition state that we have found for this process appears to agree quite well with the 'sp^3 intermediate' reported by Scuseria and co-workers[18,34], although our barrier of 500 kJ mol^{-1} is somewhat lower than theirs and closer to that obtained by Yi and Bernholc[27] for C_{60} and by Baker and Fowler[35] for C_{28}. Our calculated pathway linking the icosahedral isomer to the next lowest isomer is shown in Fig. 3.

Austin *et al.*[32] determined that the largest subset of the 1,812 C_{60} isomers which are mutually accessible via Stone–Wales rearrangements contains 1,710 minima, one of which is buckminsterfullerene. In fact, the minima can be grouped into 'stacks' according to how many Stone–Wales processes are required to convert them into buckminsterfullerene[32]. The first stack contains buckminsterfullerene itself, and the second stack contains the adjacent minimum illustrated in Fig. 3. Here we have calculated all the Stone–Wales rearrangement mechanisms up to, and including, those linking the minima in stack seven. This set includes 547 pathways, and 197 of the 1,812 local minima. We include minima only up to stack five in Fig. 4 for clarity. This figure clearly corresponds to the 'weeping willow' pattern of Fig. 1b, that is, a gentle funnel with higher barriers.

Using the above graph we have applied a master equation approach to examine the relaxation dynamics of these C_{60} isomers. A high temperature is required to produce an appreciable population of buckminsterfullerene on the experimentally observed timescales, in good agreement with the experimental observation that high-temperature annealing is needed to produce significant yields of this structure[16,36,37]. These results reflect the nature of the energy landscape revealed in Fig. 4, namely the presence of a funnel leading to the global minimum but with relatively large barriers.

Our final example is the energy landscape of a $(H_2O)_{20}$ cluster described by the TIP4P rigid-molecule effective pair potential[38]. Although this potential was designed to reproduce the properties of bulk water it can provide a useful starting point for cluster studies, despite the neglect of many-body forces. Here our objective is to explain Angell's classification of water as a 'strong' liquid in terms of the energy landscape[8,9], and a simple model with the right anisotropic form should suffice. 'Fragile' liquids have structures which change significantly with temperature, whilst 'strong' liquids often have open network structures which are preserved over relatively wide temperature ranges, and are characterized by viscosities which exhibit Arrhenius temperature dependence[8], that is, they scale as exp(constant/T) with temperature, T.

The global minimum for TIP4P $(H_2O)_{20}$ can be described in terms of three fused pentagonal prisms[39]. The graph for a sample of minima in the vicinity of this structure is shown in Fig. 5. Apart from the lowest-lying isomers, the graph resembles the 'banyan tree' shown in Fig. 1c. This pattern arises from a hierarchical structure: sets of minima are progressively connected by transition states of increasing energy, and the resulting structure is similar to that expected for a fractal[10]. Despite the wide range of transition-state energies, almost all the barrier heights are less than 20 kJ mol^{-1}, the energy of a typical hydrogen bond, and fall within a relatively narrow range. Nevertheless, the corresponding rearrangement mechanisms include both cooperative and localized processes, and the barriers are relatively large compared to the available thermal energy at temperatures where water can exist as a liquid. Global optimization for such a system is difficult because the path between a randomly chosen structure and the global minimum is likely to involve more local minima, including some of relatively high energy[39].

We have found that smaller water clusters have considerably fewer minima on the potential-energy surface than atomic Lennard–Jones clusters with the same number of degrees of freedom. We attribute this result to the longer range and anisotropy of the forces between the water molecules. The same is probably true for larger water clusters, again in agreement with previous descriptions of 'strong' liquids[40]. □

Received 20 April; accepted 8 June 1998.

1. Levinthal, C. in *Mössbauer Spectroscopy in Biological Systems, Proceedings of a Meeting Held at Allerton House, Monticello, Illinois* (eds DeBrunner, J. T. P. & Muck, E.) 22–24 (Univ. Illinois Press, Urbana, 1969).
2. Ball, K. D. *et al.* From topography to dynamics on multidimensional potential energy surfaces of atomic clusters. *Science* **271,** 963–966 (1996).
3. Wales, D. J. Tales from topographic potential surfaces. *Science* **271,** 925–929 (1996).
4. Bryngelson, J. D., Onuchic, J. N., Socci, N. D. & Wolynes, P. G. Funnels, pathways, and the energy landscape of protein folding: a synthesis. *Proteins* **21,** 167–195 (1995).
5. Doye, J. P. K. & Wales, D. J. On potential energy surfaces and relaxation to the global minimum. *J. Chem. Phys.* **105,** 8428–8445 (1996).
6. Wolynes, P. G. Symmetry and the energy landscapes of biomolecules. *Proc. Natl Acad. Sci. USA* **93,** 14249–14255 (1996).
7. Berry, R. S., Elmaci, N., Rose, J. P. & Vekhter, B. Linking topography of its potential surface with the dynamics of folding of a protein model. *Proc. Natl Acad. Sci. USA* **94,** 9520–9524 (1997).
8. Angell, C. A. Formation of glasses from liquids and biopolymers. *Science* **267,** 1924–1935 (1995).
9. Stillinger, F. H. A topographic view of supercooled liquids and glass formation. *Science* **267,** 1935–1939 (1995).
10. Becker, O. M. & Karplus, M. The topology of multidimensional potential energy surfaces: theory and application to peptide structure and kinetics. *J. Chem. Phys.* **106,** 1495–1517 (1997).
11. Wales, D. J. & Doye, J. P. K. Global optimization by basin-hopping and the lowest energy structures of Lennard–Jones clusters containing up to 110 atoms. *J. Phys. Chem. A* **101,** 5111–5116 (1997).
12. Doye, J. P. K. & Wales, D. J. Surveying a potential energy surface by eigenvector-following. *Z. Phys. D* **40,** 194–197 (1997).
13. Kroto, H. W. Space, stars, C_{60}, and soot. *Science* **242,** 1139–1135 (1988).
14. Heath, J. R., O'Brien, S. C., Curl, R. F., Kroto, H. W. & Smalley, R. E. Carbon condensation. *Comments Cond. Mat. Phys.* **13,** 119–141 (1987).
15. Heath, J. R. in *Fullerenes—Synthesis, Properties, and Chemistry of Large Carbon Clusters* (eds Hammond, G. S. & Kuck, V. J.) 1–22 (ACS Symp. Ser. 481, Am. Chem. Soc., Washington DC, 1992).
16. Smalley, R. E. Self-assembly of the fullerenes. *Acc. Chem. Res.* **25,** 98–105 (1992).
17. Endo, M. & Kroto, H. W. Formation of carbon nanofibers. *J. Phys. Chem.* **96,** 6941–6944 (1992).
18. Murry, R. L., Strout, D. L., Odom, G. K. & Scuseria, G. E. Role of sp^3 carbon and 7-membered rings in fullerene annealing and fragmentation. *Nature* **366,** 665–667 (1993).
19. Manopoulos, D. E. & Fowler, P. W. in *The Far-reaching Impact of the Discovery of C_{60}* (ed. Andreoni, W.) 51–69 (NATO ASI Ser. E **316,** Kluwer, Dordrecht, 1993).
20. Strout, D. L. & Scuseria, G. E. A cycloaddition model for fullerene formation. *J. Phys. Chem.* **100,** 6492–6498 (1996).
21. Marcos, P. A., López, M. J., Rubio, A. & Alonso, J. A. Thermal road for fullerene annealing. *Chem. Phys. Lett.* **273,** 367–370 (1997).
22. Ballone, P. & Milani, P. Simulated annealing of carbon clusters. *Phys. Rev. B* **42,** 3201–3204 (1990).
23. Chelikowsky, J. R. Nucleation of C_{60} clusters. *Phys. Rev. Lett.* **67,** 2970–2973 (1991).
24. Chelikowsky, J. R. Formation of C_{60} clusters via Langevin molecular-dynamics. *Phys. Rev. B* **45,** 12062–12070 (1992).
25. Jing, X. D. & Chelikowsky, J. R. Nucleation of carbon clusters via an accretion model. *Phys. Rev. B* **46,** 5028–5031 (1992).
26. Wang, C. Z., Xu, C. H., Chan, C. T. & Ho, K. M. Distintegration and formation of C_{60}. *J. Phys. Chem.* **96,** 3563–3565 (1992).
27. Yi, J. Y. & Bernholc, J. Reactivity, stability, and formation of fullerenes. *Phys. Rev. B* **48,** 5724–5727 (1993).
28. Xu, C. H. & Scuseria, G. E. Tight-binding molecular-dynamics simulations of fullerene annealing and fragmentation. *Phys. Rev. Lett.* **72,** 669–672 (1994).
29. Maruyama, S. & Yamaguchi, Y. A molecular dynamics demonstration of annealing to a perfect C_{60} structure. *Chem. Phys. Lett.* **286,** 343–349 (1998).
30. Porezag, D., Frauenheim, T., Seifert, G. & Kaschner, R. Construction of tight-binding-like potentials on the basis of density-functional theory—application to carbon. *Phys. Rev. B* **51,** 12947–12957 (1995).
31. Austin, S. J., Fowler, P. W., Manolopoulos, D. E., Orlandi, G. & Zerbetto, F. Structural motifs and the stability of fullerenes. *J. Phys. Chem.* **99,** 8076–8081 (1995).
32. Austin, S. J., Fowler, P. W., Manolopoulos, D. E. & Zerbetto, F. The Stone–Wales map for C_{60}. *Chem. Phys. Lett.* **235,** 146–151 (1995).
33. Stone, A. J. & Wales, D. J. Theoretical studies of icosahedral C_{60} and some related species. *Chem. Phys. Lett.* **128,** 501–503 (1986).
34. Scuseria, G. E. *Ab-initio* calculations of fullerenes. *Science* **271,** 942–945 (1996).
35. Baker, J. & Fowler, P. W. Energetics of the Stone–Wales pyracylene transformation. *J. Chem. Soc., Perkin Trans. 2*, 1665–1666 (1992).
36. Zhang, Q. L. *et al.* Reactivity of large carbon clusters—spheroidal carbon shells and their possible relevance to the formation and morphology of soot. *J. Phys. Chem.* **90,** 525–528 (1986).
37. Krätschmer, W., Lamb, L. D., Fostiropoulos, K. & Huffman, D. R. Solid C_{60}—a new form of carbon. *Nature* **347,** 354–358 (1990).
38. Jorgensen, W. L. Quantum and statistical mechanical studies of liquids. 24. Revised TIPS for simulations of liquid water and aqueous-solutions. *J. Chem. Phys.* **77,** 4156–4163 (1982).
39. Wales, D. J. & Hodges, M. P. Global minima of water clusters $(H_2O)_n$, $n \leq 21$, described by an empirical potential. *Chem. Phys. Lett.* **286,** 65–72 (1998).
40. Angell, C. A. Relaxation in liquids, polymers and plastic crystals—strong fragile patterns and problems. *J. Non-Cryst. Solids* **131–133,** 13–31 (1991).

Acknowledgements. We thank J. P. K. Doye and A. J. Stone for discussions. D.J.W., M.A.M. and T.R.W. thank the Royal Society, the EPSRC and the Cambridge Commonwealth Trust, respectively, for financial support.

Correspondence and requests for materials should be addressed to D.J.W. (e-mail: dw34@cus.cam.ac.uk).